Transport properties of lithium hydride at extreme conditions from orbital-free molecular dynamics

L. Burakovsky, C. Ticknor, J. D. Kress, L. A. Collins, and F. Lambert

Phys. Rev. E **87**, 023104 — Published 13 February 2013

DOI: 10.1103/PhysRevE.87.023104

Transport properties of lithium hydride at extreme conditions from orbital free molecular dynamics

L. Burakovsky, C. Ticknor, J..D. Kress, and L.A. Collins
Theoretical Division, Los Alamos National Laboratory, Los Alamos, New Mexico 87545

F. Lambert
CEA, DAM, DIF, F-91297 Arpajon,France

We have performed a systematic study of lithium hydride (LiH), using orbital-free molecular dynamics, with a focus on mass transport properties such as diffusion and viscosity by extending our previous studies at the lower end of the warm, dense matter regime to cover a span of densities from ambient to ten-fold compressed and temperatures from 10 eV to 10 keV. We determine analytic formulas for self- and mutual-diffusion coefficients, and viscosity, which are in excellent agreement with our molecular dynamics results, and interpolate smoothly between liquid and dense plasma regimes. In addition, we find the orbital-free calculations begin to agree with the Brinzinskii-Landau formula above about 250 eV at which point the medium becomes fully ionized. A binary-ion model based on a bare Coulomb interaction within a neutralizing background with the effective charges determined from a regularization prescription shows good agreement above about 100 eV with the orbital-free results. Finally, we demonstrate the validity of a pressure-based mixing rule in determining the transport properties from the pure-species quantities.

PACS numbers:

I. INTRODUCTION

The area of warm, dense matter (WDM) and high energy density physics (HEDP) [1] has received considerable attention recently due its identification with an assortment of environments as diverse as the interiors of exoplanets[2], the atmospheres of stars[3], inertial confinement fusion capsules[4], and the plasma from laser interactions[5] with materials from clusters to nanostructures that span temperatures from a few thousand ($\sim$1 eV) to a few million ($\sim$100 eV) degrees Kelvin and densities from a few hundredths solid ($\sim 10^{21}$atoms/cm^3) to hundreds of times compressed solid ($\sim 10^{25}$atoms/cm^3). The WDM regime presents a particularly difficult challenge given that quantum mechanical effects play a crucial role in the accurate representation of this complex medium under extreme conditions. In addition, many of these environments constitute the dynamical interplay of mixtures of species in various physical states. While studies have addressed various aspects of mixtures in particular WDM and HEDP cases, few systematic studies exist that examine the efficacy of various models over an extended range of densities and temperatures.

In our earlier studies[6, 7] on lithium hydride (LiH), we explored the lower end of the WDM regime (2eV $<$ T$<$ 10eV and $\rho/\rho_0 \leq 4$, where ρ_0 is the ambient solid density) with quantum molecular dynamics (MD) simulations employing finite-temperature versions of the two major flavors of density functional theory (DFT), namely orbital-based Kohn-Sham (KS) and orbital-free (OF). We found reasonable agreement between the the two schemes for equation-of-state, mass transport, and optical properties. However, the computational intensity of the KS-DFT placed severe limitations on further extensions into the WDM regime indicating that the OFMD approach[8–11], particularly based on the Thomas-Fermi-Dirac form, would serve as the principal vehicle for exploring the gulf between warm liquids and fully-ionized plasmas. Other OFMD studies on a variety of pure species such as hydrogen[9], aluminum[10], iron[10, 11], boron[12], uranium[13], and plutonium[14] and of mixtures, including deuterium/copper[15], aluminum/gold[16], and deuterium/tritium[17] support this observation. To this end, we have extended our investigation of mixtures, using LiH as a representative candidate, with the OFMD formulation across a broad swath of extreme conditions in the WDM and HEDP regimes comparing against other approaches where appropriate. We focus on dynamical properties such as diffusion and viscosity.

II. FORMALISM

In this section, we present a brief description of the basic formalism employed to treat mixtures in the WDM regime given that more comprehensive discussions appear elsewhere as indicated in the citations. The OFMD approach forms the basis of our simulations. We also discuss the implementation of various schemes to determine the dynamical properties such as diffusion and viscosity. The final part treats the mixing rules that combine pure species quantities to form properties of the composite system.

A. Orbital Free Molecular Dynamics

We consider a a cubic volume V (=L^3) containing N$_H$ hydrogen atoms of mass m$_H$ and N$_{Li}$ lithium atoms of mass m$_{Li}$ with total number and mass densities given

by n = (N_H + N_{Li})/V and ρ = ($m_H N_H$ + $m_{Li} N_{Li}$)/V respectively and the concentrations by x_α = N_α/N, N= N_H + N_{Li}. In OFMD simulations [9, 10, 12, 15] the kinetic energy of the electrons is treated in a semiclassical approximation, up to first order in the partition function of the electrons. The orbital-free procedure treats all electrons on an equal footing, albeit approximately, with no distinction between bound and ionized electrons. The orbital-free electronic free energy at ion positions $\mathbf{R}$ is given by

$$\begin{aligned} & F_e\big[\mathbf{R}, n_e\big] = \qquad (1) \\ & +\frac{1}{\beta}\int \mathrm{d}\mathbf{r}\left(n_e(\mathbf{r})\Phi[n_e(\mathbf{r})] - \frac{2\sqrt{2}}{3\pi^2\beta^{\frac{3}{2}}} I_{\frac{3}{2}}\big(\Phi[n_e(\mathbf{r})]\big)\right) \\ & + \int \mathrm{d}\mathbf{r}\, V_{ext}(\mathbf{r}) n_e(\mathbf{r}) + \frac{1}{2}\iint \mathrm{d}\mathbf{r}\mathrm{d}\mathbf{r}'\, \frac{n_e(\mathbf{r}) n_e(\mathbf{r}')}{|\mathbf{r}-\mathbf{r}'|} \\ & + F_{xc}[n_e] \end{aligned}$$

where $\beta = 1/k_B T$. T is the temperature, k_B is the Boltzmann's constant, and I_ν is the Fermi integral of order ν. The screened potential $\Phi[n_e(\mathbf{r})]$ is related to the electronic density $n_e(\mathbf{r})$ by [15]

$$n_e(\mathbf{r}) = \frac{\sqrt{2}}{\pi^2\beta^{\frac{3}{2}}}\, I_{\frac{1}{2}}\big(\Phi[n_e(\mathbf{r})]\big) \qquad (2)$$

with charge conservation constraining the integral $\int d\mathbf{r}\, n_e(\mathbf{r})$ to be equal to the total electronic charge.

The first integral in Eq.1 is the finite-temperature Thomas-Fermi expression [18]. The other terms in Eq. (1) represent the external or electron-ion interaction, the Hartree contribution to the electronic energy, and the exchange-correlation potential. The exchange-correlation term $F_{xc}[n_e]$ is expressed in the local density approximation of Perdew and Zunger [19, 20]. For this study, we omit the von Weiszäcker correctionand work in a Thomas-Fermi-Dirac form using the formula proposed by Perrot [22] to represent the kinetic-entropic part. We have made spot checks and found that the von Weiszäcker correction term gives only small corrections ($< 5\%$) in the regimes examined. This coincides with the conclusions of a few other studies, for example [21]. The divergence of the electron-nucleus potential is regularized at each thermodynamic condition [11]. The cutoff radius is chosen to be 30% of the Wigner-Seitz radius, sufficient to prevent overlap of the regularization spheres. The number of plane waves describing the local electronic density is then adjusted to converge the thermodynamic properties to within 1%. This usually requires a energy cut off of 400eV.

At each time step, the electronic free energy is minimized in terms of the local electronic density. The ions are evolved classically according to the forces due to the electron density and the ion-ion repulsion. The system is assumed to be in local thermodynamic equilibrium with the electron and ion temperatures equal ($T_e = T_i = T$). In our simulations, the electron temperature is fixed, and the ion temperature is kept at this value through an isokinetic thermostat applied to each species[23].

We also perform simulations with a binary ion model (BIM), which serves as the two-species analogue of the usual one-component plasma scheme. In this case, the ions interact through a Coulomb potential [$Z_\alpha Z_\beta/r$; r the inter-particle distance] with the electrons serving as a static neutralizing background. However, the effective charge Z_α comes from the ionization degree determined by the regularization prescription [11] for the pure species (i) rather than the bare ion charge.

B. Static and Transport Properties

In this section, we present only a brief summary of the basic static and dynamical properties determined in our simulations since detailed expositions appear elsewhere [24–26].

The total pressure of the system

$$P = n k_B T + P_e \qquad (3)$$

is the sum of the ideal gas pressure of the ions and the electron pressure P_e, computed via the electronic forces from the DFT calculation and averaged over the trajectory after the system has equilibrated.

The self-diffusion coefficient D_α for species α is computed from the trajectory for the mean square displacement

$$D_\alpha = \frac{1}{6t}\Big\langle \big|\mathbf{R}_i(t) - \mathbf{R}_i(0)\big|^2 \Big\rangle \qquad (4)$$

or by the velocity autocorrelation function

$$D_\alpha = \frac{1}{3}\int_0^\infty \big\langle \mathbf{V}_i(t)\cdot\mathbf{V}_i(0)\big\rangle\, \mathrm{d}t\ , \qquad (5)$$

where $\mathbf{R}_i$ ($\mathbf{V}_i$) is the position (velocity) of the i-th particle of species α.

We computed the mutual diffusion coefficient $D_{\alpha\beta}$ from the autocorrelation function

$$D_{\alpha\beta} = \frac{Q}{3N x_\alpha x_\beta}\int_0^\infty \big\langle A(0)A(t)\big\rangle\, \mathrm{d}t \qquad (6)$$

with

$$A(t) = x_\beta \sum_{i=1}^{N_\alpha} \mathbf{v}_i(t) - x_\alpha \sum_{j=1}^{N_\beta} \mathbf{v}_j(t)\,. \qquad (7)$$

We set the thermodynamic factor Q to unity[27], the value for mixtures of ideal gases, although many other systems and conditions warrant this choice[25, 28]. For charged systems, Q can have both concentration and weak-temperature dependencies[29]. If the interspecies interactions remain small compared to the intraspecies ones, then the mutual diffusion coefficient takes a very

simple form in terms of the concentrations and the self-diffusion coefficients:

$$D_{\alpha\beta} = x_\beta D_\alpha + x_\alpha D_\beta. \tag{8}$$

This relation does not correspond to a standard mixing rule as described in the next section since the self-diffusion coefficients arise from simulations on the *full* mixture not on each pure species.

The viscosity was computed from the autocorrelation function of the off-diagonal component of the stress tensor[24]

$$\eta = \lim_{t\to\infty} \overline{\eta}(t), \tag{9}$$

where

$$\overline{\eta}(t) = \frac{V}{k_B T} \int_0^t \left\langle P_{12}(0) P_{12}(t') \right\rangle \, \mathrm{d}t'. \tag{10}$$

We averaged the results for the five independent off-diagonal components of the stress tensor P_{xy}, P_{yz}, P_{zx}, $(P_{xx} - P_{yy})/2$, and $(P_{yy} - P_{zz})/2$.

We have found that the use of empirical fits to the integrals of the autocorrelation functions can substantially shorten the length of the trajectory required. The basic mechanics of this procedure appear in detail elsewhere[7, 17]. The statistical error inherent in computing correlation functions from molecular dynamics trajectories[30] is $\sqrt{2\tau/N_t\delta_t}$, where $N_t\delta_t$ is the length of the trajectory and τ is the correlation or e-folding time of the autocorrelation function, calculated either directly from the fit or from an interrogation of the function itself. We generally fit over a time interval of $[0,(4-5)\tau]$. For the viscosity and mutual diffusion coefficients, the error computed in this way is 30% or less. On the other hand, the error for the self-diffusion remains at less than 5%, since the particle average introduces an additional factor of $1/\sqrt{N}$.

We follow Clerouin *et al.* [31] and fit the transport properties Λ to an expansion of the form

$$\Lambda = T^{5/2} \exp\left(a + b\ln x + c\ln^2 x \; + d\ln^3 x\right), \tag{11}$$

where $x \equiv \rho/T^3$. Their motivation arose from the observation that $\eta\cdot(1/T)^{1/2+2/n}$ is a universal function of $\rho T^{-3/n}$ for systems with inverse interaction potentials of order n. They noticed that with $n = 1$ (bare Coulomb potential), the above formula fits the results of their classical molecular dynamics simulations extremely well for the viscosity ($\Lambda = \eta$). We introduce a slight modification by including terms up to $\ln^3 x$ and suggest an analog for diffusion coefficients $\Lambda = \rho D$, based on the fact that dimensionality of D coincides with that of η/ρ. The results of these fits for the transport properties are given in Table I, so that the units are cm^2/s for D, $mPas$ for η, eV for T, and g/cm^3 for ρ.

At a temperature sufficiently high to fully ionize the medium, the viscosity should follow the Braginskii-Landau formula[31, 32]

$$\frac{\eta}{\eta_{\rm pl}} = -\frac{5}{6}\,\frac{\pi^{1/2}}{3^{1/2}\,\Gamma^{5/2}\,\ln(3^{1/2}\,\Gamma^{3/2})}, \tag{12}$$

where $\eta_{\rm pl}$ is the characteristic plasma viscosity and Γ is the Coulomb coupling parameter. With T in eV and ρ in g/cm^3, Eq.(12) becomes

$$\eta = 3.85\times10^{-3}\,\frac{T^{5/2}\,A^{1/2}}{Z^4\,\ln\left\{\frac{T^{3/2}\,A^{1/2}}{3^{1/2}\,19.6^{3/2}\,Z^3\,\rho^{1/2}}\right\}}\;\;\mathrm{mPa\cdot s}, \tag{13}$$

where A is the atomic weight and Z is the atomic number. For LiH, we used $A = 4$ and $Z = 2$, from a linear mixing $A = x_1A_1 + x_2A_2$ and $Z = x_1Z_1 + x_2Z_2$.

C. Mixing Rules

We also test the validity of mixing rules for determining the properties of the composite from combinations of those from the pure species. Previous studies[6, 7, 15, 16] have found that prescriptions based on matching pressures generally produce better agreement with results for the full system. In this procedure for a fixed system volume $V_{\rm LiH}$ and number of particles $N_{\rm LiH} = N_{\rm H} + N_{\rm Li}$, we must perform a series of OFMD simulations on the individual species in which their volumes $[V_\alpha]$ with a fixed number of particles $[N_\alpha]$ are varied under the constraint $[V_{\rm LiH} = V_{\rm H} + V_{\rm Li}]$ until the individual electronic pressures agree $[P_e^{\rm H} = P_e^{\rm Li}]$. (This procedure is also know as additive volume and Amagat mixing.) Composite properties such as mutual diffusion and viscosity are determined by combining the individual species results according to the volume fractions $[v_\alpha = V_\alpha/V_{LiH}]$.

$$D_{\rm LiH} = v_{\rm H}D_{\rm H} + v_{\rm Li}D_{\rm Li} \tag{14}$$

$$\eta_{\rm LiH} = v_{\rm H}\eta_{\rm H} + v_{\rm Li}\eta_{\rm Li}. \tag{15}$$

As an aside, applying the mixing rule with the total pressure, instead of the electronic pressure, gives similar results. The partial volumes are different but in the end the results are in good agreement with the mixing rule based on the electronic pressure and the fully mixed simulations.

These mixing rules offer a faster method to get transport properties over a wider range of parameters than the fully mixed simulations. Pure simulations are more efficient than mixed ones, because they can be run at an appropriate time step for the species being studied. In contrast, the fully-mixed simulation time step must be run at the shorter time step, but for the duration of the longer simulation to resolve the properties. Additionally, mixing rules are based on interpolated properties so to build up a collection of data spanning a wide range of parameters requires fewer simulations. Furthermore, the mixing rules can be applied to different mixture ratios, whereas, the full simulations have to be rerun to get such data.

III. RESULTS AND DISCUSSION

A. Simulation details

We present the wealth of information derived from our calculations mainly through tables and figures and concentrate in the text on general trends and representative cases. We explore LiH mixtures in a regime of more extreme conditions than our previous studies [6, 7] and examine densities from 1 to 10 times solid density, $\rho_0 = 0.788$ g/cm^3, and temperatures from 10 eV ($\sim$100 kK) to 10 keV ($\sim$100 MK). Before analyzing the results of the OFMD calculations, we focus on several procedural points that underlie the computation of the various static and dynamical properties.

In each of the 70 cases studied, we treated a system of 128 (64H+64Li) atoms initially arranged into a $4 \times 4 \times 4$ B2 (CsCl-type) cubic lattice with a lattice constant corresponding to a given density. The system was then subjected to a given temperature and run for a total time of order 1 ps. The size of a time step, δt in each case was calculated using the scaling form $\delta t \sim 1/(\rho^{1/3} T^{1/2})$, based on the values of δt for densities (1-4)$\times\rho_0$ and temperatures (2-6) eV used in our previous studies. [7]. The total number of time steps, N_t, was between $\sim 10^4$ (for a δt of order 0.1 fs) and $\sim 10^5$ (for a δt of order 0.01 fs).

B. Properties

1. Pressure

In Figure 1, we present the electronic (excess) pressure P_e of the LiH mixture as a function of compression and temperature. As anticipated, these rise monotonically with increasing density and temperature.

2. Transport properties

Before discussing the behavior of the various transport properties over the WDM and HEDP terrain, we focus on a representative case in order to elucidate some common features, in particular, LiH at three times solid density (2.364 g/cm^3) and temperatures from a few eV to a few keV as depicted in Fig. 2. The simulations for the OF-DFT and KS-DFT agree well at low temperatures as discovered in our earlier studies[7]. The modified BIM also shows relatively good agreement by about 100eV although even at 10eV the difference with OFMD is only a factor of two. We note that the BIM was implemented using effective charges derived from the regularization so that some account of the degree of ionizations appears. Above about 250eV, the OFMD begins to agree with the Braganskii-Landau form, which seems reasonable given that the system reaches total ionization above 100eV. Even above this point, the electrons still have a dynamic component that responds to and partially shields the ions. The basic picture though seems clear in that the OFMD can serve as an effective and efficient technique for spanning between regimes dominated by quantum or classical mechanics.

In Figs. 3 and 4, we present the self-diffusion coefficients for hydrogen (D_H) and lithium (D_{Li}) as a function of density and temperature. The colored dots display the OFMD simulation results while the lines represent the fit in Eq.(11) with parameters given in Table I. The fit gives a reasonable reproduction of the results to within 20% or less of the OFMD values above 25 eV for all densities. For a fixed density, the self-diffusion coefficient rises with temperature as the atoms become more mobile. On the other hand, for a given temperature, the diffusion declines with increasing density, reflecting the greater confinement of the atoms. Throughout the entire temperature range, the hydrogen diffusion is faster. The ratio of the hydrogen diffusion to that of lithium starts at about three for the lower temperatures and steadily climbs to a value of about fifteen to twenty above about 100 eV remaining at this value up to 10 keV. This plateau in the ratio roughly corresponds to the point at which the system becomes fully ionized. Calculations using the regularization prescription for Li give an effective ionization of about 50% at 20 eV and almost 100% by 200 eV. The trend in the ratio with temperature demonstrates little sensitivity to density.

The statistical errors in viscosity are smaller than 10% for T up to 500 eV at all compression, and smaller than 40% for: $T = 1-2$ keV at compressions 1-3; $T = 1-3.5$ keV at compression 5; and $T = 1-5$ keV at compression 10. For higher T, errors increase drastically: up to 90% for $T = 5-10$ keV at compressions 1-3; up to 85% for $T = 5-10$ keV at compression 5; and up to 75% for $T = 10$ keV at compression 10. The reason for such a large increase in the error is limitation in the simulation length. For example, in the ($T = 1$ keV,$\rho/\rho_0 = 1$) case, N_t =330000 with δ_t =0.02 fs produced an error of 90%. In order to reduce it to 50%, a simulation of one million time steps is needed, which is infeasible to do. Hence, for practical reasons, there is a temperature limit of OFMD simulations, beyond which the errors increase drastically; in the LiH case it corresponds to temperatures of order 1 keV. Nevertheless, we can demonstrate the results which correspond to larger error bars are reliable. We fit Eq. (11) to our results for which error bars remained within 40%, and determined a new set of coefficients a_i. We then applied Eq. (11) with the new a_i to calculate viscosity in cases where error bars were 75-90%, and in each such case the new values where within 15% of the original values.

In Figs. 5 and 6, we display the viscosity and mutual diffusion coefficients as a function of density and temperature. The colored dots display the OFMD simulation results while the lines represent the fit in Eq.(11) with parameters given in Table I. The fit gives a reasonable reproduction of the results to within 25% or less of the

OFMD values above 25 eV for all densities. Not surprisingly, the general trends in density and temperature follow those of the self-diffusion coefficients as discussed in the previous section. In addition, we find that the mutual diffusion coefficient agrees with Eq.(8) at the 15% level for lower temperatures ($T \leq 500$ eV) but departs by as much as 50% for higher temperatures. This indicates that the H-Li correlations become more important as the temperature rises.

Fig. 7 shows that our OFMD results agree with the Braginskii-Landau formula for temperature above 250 eV. This can be interpreted as LiH becomes fully ionized and the density dependence of the "exact" ionization temperature is rather weak. The results from the regularization procedure, as mentioned above, support this observation as does an argument based on the virial theorem along the principal Hugoniot [33, 34].

As an interesting aside, we note that Eq. (11) reproduces the experimental value of the viscosity of LiH at ambient conditions. Namely, the LiH viscosity above its ambient melting point ($\rho = \rho_0$, T=0.1 eV) is 0.535 mPa$\cdot$s, which agrees with the experimental value 0.539 mPa$\cdot$s at 1150 K [35]. The formula, which describes the results of OFMD simulations, appears to extrapolate smoothly to the liquid region and reproduces experimental ambient viscosity values, not only for LiH but also for aluminum, uranium, and plutonium [36]. Perhaps, the general physical nature of the functional form deserves a further detailed study.

C. Mixing rules

We apply a mixing rule to obtain an estimate of the transport properties of a fully mixed LiH system. In order to simplify the search for the matching the electronic pressures as detailed in section II.C, we perform a series of OFMD calculations for the pressures and viscosities of the pure species across a range of temperatures and densities. For a fixed temperature, the property as a function of density (volume) is fit to the simple form $a\rho^b$; the results appear in Table II and are displayed in Fig. 8 for the electronic pressure. We vary the densities of each species until the electronic pressures match [$P_e^{\rm H} = P_e^{\rm Li}$], which sets the volume fractions v_i. Then from the prescription in Eq.(15) and the single-species transport properties at these conditions, we determine the mixture viscosity or diffusion. The electronic pressures for both Li and H are in Fig. 8 are shown, as are the linear fits used in the mixing rule. Comparing the electronic pressure from the mixing rule and the full simulation, we typically find excellent agreement at 1% level.

Fig. 9 shows the viscosity obtained from the mixing rule (solid lines) and the fully mixed simulation (full circles) for 10 (black dots), 40 (red triangles), and 100 (blue squares) eV. At low temperatures the mixing rule gives very good estimates of the viscosity. At the highest temperature tested, 100 eV, the agreement is not as good as the lower temperatures. The mixing rule over-estimates systematically by about 20%; however the agreement is still reasonable considering the $\sim 30\%$ error bars of the full simulations. Additionally, the fits from Eq. (11) are shown as dashed lines for each temperature. These fits do a very good job of reproducing the data as a function of temperature and compression. At the higher temperature, the fits are slightly lower than the data and therefore lower than the estimate of the mixing rule.

Fig. 10 shows the mutual diffusion obtained from the mixing rule (solid lines) and the full simulation for 10 (black dotes), 40 (red triangles), and 100 (blue squares) eV. The mixing rule reproduces the fully mixed simulation results very well across the whole temperature range. The fits from Eq. (11) are shown as dashed lines for each temperature. These fits do a very good job of reproducing the data as a function of temperature and compression. An interesting trend is that at the highest temperature the fit seems systematically high compared to the data and mixing rule.

Figs. 9 and 10 show that the mixing rule is a good means to estimate transport properties of LiH; especially if the mixture ratios are different than the presented full simulations.

IV. SUMMARY

We have performed a systematic study of lithium hydride (LiH) in the warm-dense-matter (WDM) regime for a density range from one to ten times ambient solid density and for temperatures from 10 eV to 10 keV, using orbital free molecular dynamics (OFMD) simulations. The study concentrated on dynamical properties such as diffusion and viscosity. We suggested analytic formulas for self- and mutual-diffusion coefficients, and viscosity of LiH, which are in excellent agreement with our OFMD results, and interpolate smoothly between liquid and WDM regimes. We showed that at temperatures above 250 eV, our results on the viscosity of LiH approach theoretical predictions provided by the Braginskii-Landau formula for a fully-ionized plasma. Furthermore, we studied mixing rules between 10 and 100 eV over a wide range of compressions. We found good agreement between these estimates and the fully mixed simulation results. Finally, we presented mixing rules results to the transport properties, and found that these methods provide a good estimate for the fully mixed transport properties. They provide an efficient method to estimate such properties over a wider range of parameters than presented here.

Acknowledgments

The Los Alamos National Laboratory is operated by Los Alamos National Security, LLC for the National Nuclear Security Administration of the U.S. Department of Energy under Contract No. DE-AC52-06NA25396. This

work was part of an international agreement on cooperation in fundamental science supporting stockpile stewardship between the CEA/DAM and DOE/LANL; collaboration P184.

[1] R. P. Drake, Physics Today **63**, 28 (2010).

[2] N.C. Santos, W. Benz, and M. Mayor, Science **310**, 251 (2005); A. Burrows, Nature **433**, 261 (2005). N.C. Santos, W. Benz, and M. Mayor, Science **310**, 251 (2005); A. Burrows, Nature **433**, 261 (2005).

[3] G. Fountaine, P. Brassard, and P. Bergeron, Publ. Astron. Soc. Pac. **113**, 409 (2001).

[4] B.A. Hammel, S.W. Haan, D.S. Clark, M.J. Edwards, S.H Langer *et. al.*, High Energy Density Phys. **6**, 171 (2010).

[5] K. Widmann, T. Ao, M. Foord, D. Price A. Ellis, P. Springer, and A. Ng, Phys. Rev. Lett. **92**, 125002 (2004).

[6] D.A. Horner, J.D. Kress, and L.A. Collins, Phys. Rev. B **77**, 064102 (2008).

[7] D.A. Horner, F. Lambert, J.D. Kress, and L.A. Collins, Phys. Rev. B **80**, 024305 (2009).

[8] G. Zérah, J. Clérouin and E. L. Pollock, Phys. Rev. Lett. **69**, 446 (1992).

[9] J. Clérouin, E. L. Pollock, and G. Zérah, Phys. Rev. A **46**, 5130 (1992).

[10] F. Lambert, J. Clérouin and S. Mazevet, Eur. Phys. Lett. **75**, 681 (2006).

[11] F. Lambert, J. Clérouin and G. Zérah, Phys. Rev. E **73**, 016403 (2006).

[12] S. Mazevet, F. Lambert, F. Bottin, G. Zérah, and J. Clérouin, Phys. Rev. E **75**, 056404 (2007).

[13] J. D. Kress, J. S. Cohen, D. P. Kilcrease, D. A. Horner, and L. A. Collins, High Energy Density Phys. **3**, 155 (2011)

[14] J. D. Kress, J. S. Cohen, D. P. Kilcrease, D. A. Horner, and L. A. Collins, Phys. Rev. E **83**, 026404 (2011)

[15] F. Lambert, J. Clérouin, J.-F. Danel, L. Kazandjian, and G. Zérah, Phys. Rev. E **77**, 026402 (2008).

[16] J. Clerouin, V. Recoules, S. Mazevet, P. Noriret, and P. Renaudin, Phys. Rev. B **76**, 064204 (2007).

[17] J. D. Kress, J. S. Cohen, D. A. Horner, F. Lambert, and L. A. Collins, Phys. Rev. E **82**, 036404 (2010).

[18] M. Brack and R. K. Bhaduri, *Semiclassical Physics* (Westview Press, Boulder, CO, 2003).

[19] J. P. Perdew and A. Zunger, Phys. Rev. B **23**, 5048 (1981).

[20] G. Faussurier, P. L. Silvestrelli, and C. Blancard, High Energy Density Phys. **5**, 74 (2009).

[21] J. Clerouin and S. Bernard, Phys. Rev. E **56**, 3534 (1997); J. F. Danel and L. Kazandjian and G. Zerah, Phys. Plasmas,**15**, 072704 (2008).

[22] F. Perrot, Phys. Rev. A **20**, 586 (1979).

[23] P. Murray, G.J. Martyna, and M.E. Tuckerman, J. Chem. Phys. **118**, 2510 (2003).

[24] M. P. Allen and D. J. Tildesley, *Computer Simulation of Liquids* (Oxford University Press, New York, 1989).

[25] M. Schoen and C. Hoheisel, Mol. Phys. **1**, 33 (1984)

[26] D. Alfe and M.J. Gillan, Phys. Rev. Lett. **23**, 5161 (1998)

[27] J.-P. Hansen and I.R. McDonald, *Theory of Simple Liquids* (Academic Press, New York, 1986), p288.

[28] J.P Hansen, F. Jolly, and I.P. McDonald, Physica, **132A**, 472 (1986).

[29] D.B. Boercker and E.L. Pollack, Phys. Rev. A **36**, 1779 (1987).

[30] R. Zwanzig and N.K. Ailawadi, Phys. Rev. **182**, 280 (1969)

[31] J.G. Clérouin, M.H. Cherfi, and G. Zérah, Europhys. Lett. **42**, 37 (1998); J.-F. Dufrêche and J. Clerouin, J. Phys. IV France **10**, Pr5-303 (2000)

[32] L. Spitzer, Jr. *Physics of Fully Ionized Gases,* 2nd edition (Interscience Publishers, 1967), p. 143; S. Ichimaru, *Basic Principles of Plasma Physics,* (Benjamin, New York, 1973)

[33] J.D. Johnson, Phys. Rev. E **59**, 3727 (1999)

[34] S. Eliezer, A. Ghatak, and H. Hora, *Fundamentals of Equations of State,* (World Scientific, 2002), p. 131

[35] E.E. Shpil'rain *et al., Thermophysical Properties of Lithium Hydride, Deuteride, and Tritide and of Their Solutions with Lithium*, AIP, New York, 1987, p. 148

[36] L. Burakousky *et al.*, unpublished.

function	a	b	c	d
η	-6.34716 [-1]	7.44564 [-1]	1.74637 [-2]	7.64182 [-5]
ρD_{LiH}	-4.72311 [0]	6.17823 [-1]	1.31917 [-2]	6.95726[-5]
ρD_{Li}	-5.52142 [0]	5.28932 [-1]	-4.69543 [-3]	-4.29052 [-4]
ρD_H	-4.72117 [0]	4.98225 [-1]	3.799 [-3]	-1.86214 [-4]

TABLE I: Fitting coefficients for the viscosity and the mutual and self diffusion coefficients in Eq.(11) with ρ in g/cm^3, T in eV, η in mPa s, and D in cm^2/s. The number in square brackets indicate the power of 10 multipling the number.

TABLE II: Fitting parameters to the form aρ^b for the pure species pressures, total (P) and electronic (P_e), viscosities (η), and self-diffusion coefficients (D) as a function of mass density(g/cm^3) at specific temperatures.

	T [eV]	a^H	b^H	a^{Li}	b^{Li}
P[GPa]	10	1880.6	1	429.86	1
P_e[GPa]	10	914.85	1	290.65	1
η[mPas]	10	5.481	0.151242	2.3890	0.21197
D[cm^2/s]	10	0.09328	-0.8270	0.04131	-0.81973
P[GPa]	50	9047.07	1	2171.8	1
P_e[GPa]	50	4229.68	1	1476.15	1
η[mPas]	50	54.95	0.3262	8.8611	0.4506
D[cm^2/s]	50	0.8515	-0.7201	0.1580	-0.588852
P[GPa]	100	18838.1	1	4787.84	1
P_e[GPa]	100	8989.57	1	3397.73	1
η[mPas]	100	175.083	0.3262	20.0861	0.356338
D[cm^2/s]	100	2.47636	-0.7201	0.319285	-0.60311

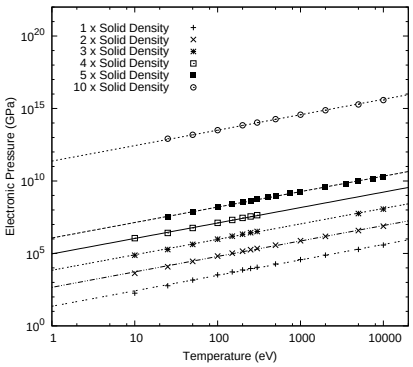

FIG. 1: (color online) Electronic pressures as a function of temperature, for six isochores of $\rho = \rho_0 \times$ [1 (+) , 2 (x), 3 (star), 4 (open square), 5 (square), and 10 (circle)]. The isochore $\rho = n \times \rho_0$ is shifted by $(n-1)$ decades relative to the isochore for ρ_0 (=0.788g/cm^3).

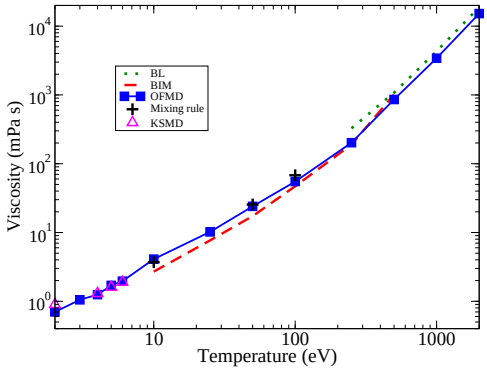

FIG. 2: (color online) Comparison of the viscosity at $\rho = 3 \times \rho_0$ as a function of temperature for several models: KSMD (magenta triangles); OFMD (blue square with solid line); BIM (dashed red line red); and Braginksii-Landau (green dotted line)

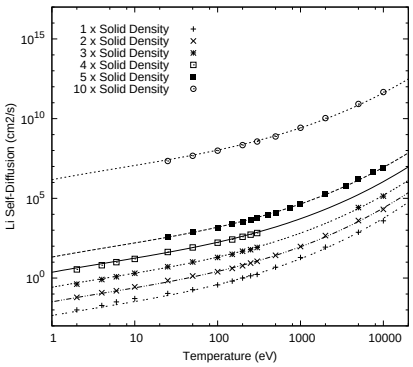

FIG. 3: (color online) Comparison of self-diffusion coefficient for Li as a function of temperature, for six isochores of $\rho = \rho_0 \times$ [1 (+) , 2 (x), 3 (star), 4 (open square), 5 (square), and 10 (circle)] to the fit of the simulations from Eq. (11). The isochore $\rho = n \times \rho_0$ is shifted by $(n-1)$ decades relative to the isochore for ρ_0.

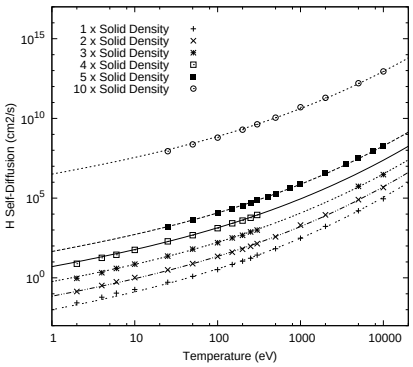

FIG. 4: (color online) Comparison of self-diffusion coefficient for H as a function of temperature, for six isochores of $\rho = \rho_0 \times$ [1 (+) , 2 (x), 3 (star), 4 (open square), 5 (square), and 10 (circle)] to the fit of the simulations from Eq. (11). The isochore $\rho = n \times \rho_0$ is shifted by $(n-1)$ decades relative to the isochore for ρ_0.

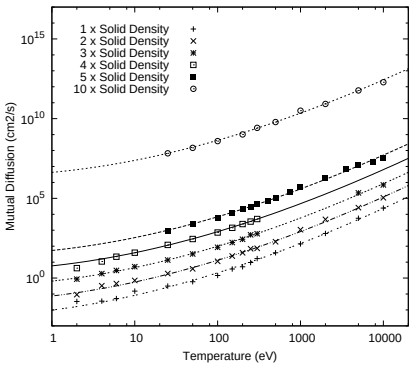

FIG. 5: (color online) Comparison of LiH mutual diffusion coefficient as a function of temperature, for six isochores $\rho = \rho_0 \times$ [1 (+) , 2 (x), 3 (star), 4 (open square), 5 (square), and 10 (circle)] to the fit of the simulations from Eq. (11). The isochore $\rho = n \times \rho_0$ is shifted by $(n-1)$ decades relative to the isochore for ρ_0.

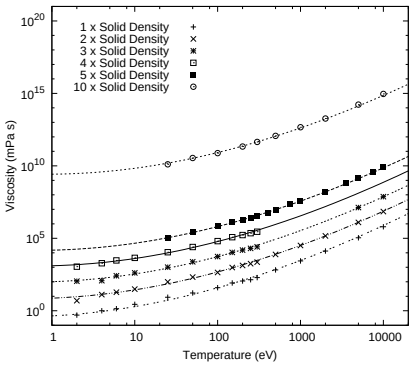

FIG. 6: (color online) Comparison of LiH viscosity as a function of temperature, for six isochores $\rho = (1, 2, 3, 4, 5, 10) \times \rho_0$, to the fit of the simulations from Eq. (11). The isochore $\rho = n \times$ Solid is shifted by $(n-1)$ decades relative to the isochore for ρ_0.

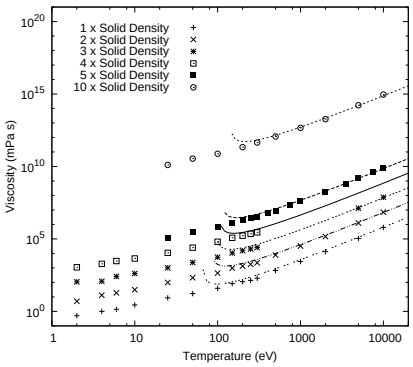

FIG. 7: (color online) Comparison of LiH viscosity as a function of temperature, for six isochores of $\rho = \rho_0 \times$ [1 (+) , 2 (x), 3 (star), 4 (open square), 5 (square), and 10 (circle)] to the Braginskii-Landau formula, Eq. (12). The isochore $\rho = n \times \rho_0$ is shifted by $(n-1)$ decades relative to the isochore for ρ_0.

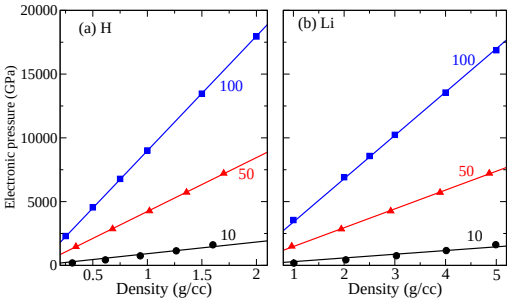

FIG. 8: (color online) The electronic pressure of pure H (a) and pure Li (b) as a function of density for T: 10 (black dots), 50 (red triangles), and 100 (blue squares) eV. The calculated pressure is shown as points and a linear fit as a solid line.

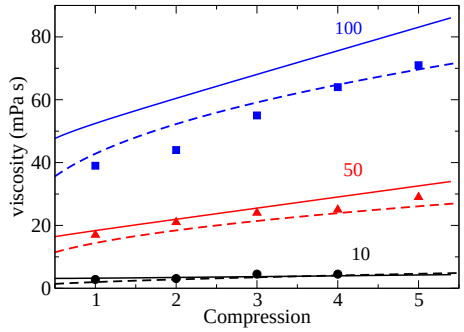

FIG. 9: (color online) The viscosity the full LiH simulations (points) and mixing rule (lines) as a function of compression for T: 10 (black dots), 50 (red triangles), and 100 (blue squares) eV from bottom to top. The fits to the fully mixed simulations from Eq. (11) are shown as dashed lines.

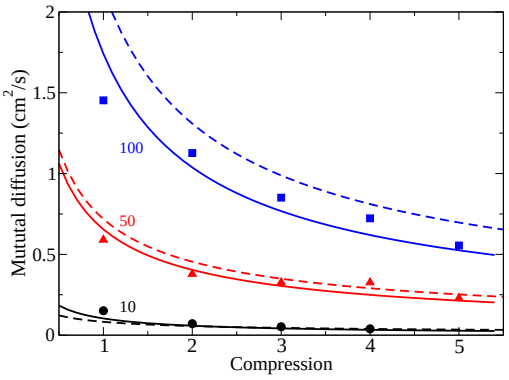

FIG. 10: (color online) The mutual diffusion coefficients for the full LiH simulations (points) and mixing rule (lines) are shown as a function of compression for T: 10 (black dots), 50 (red triangles), and 100 (blue squares) eV from bottom to top. The fits to the fully mixed simulations from Eq. (11) are shown as dashed lines.